

Probing the switching mechanism in ZnO nanoparticle memristors

Cheng Li, Gareth J. Beirne¹⁾, Gen Kamita, Girish Lakhwani, Jianpu Wang^{2, a)} and Neil C. Greenham^{a)}

Cavendish Laboratory, J. J. Thomson Avenue, Cambridge CB3 0HE, United Kingdom

Abstract:

We investigate the resistance switching mechanism in memristors based on colloidal ZnO nanoparticles using electroabsorption (EA) spectroscopy. In this EA experiment, we incorporate a small amount of low-bandgap polymer, poly(9,9-dioctylfluorene-*co*-benzothiadiazole) (F8BT), as a probe molecule in ZnO-nanoparticle memristors. By characterizing this polymer, we can study the change of built-in potential (V_{BI}) in the device during the resistance switching process without disturbing the resistance state by the EA probe light. Our results show that V_{BI} increases when the device is switched to the high resistance state, suggesting a shift of effective workfunction of the electrode. Thus, we attribute the resistance switching to the field-dependent migration of oxygen vacancies associated with the adsorption and desorption of oxygen molecules at the Al/ZnO interface. This process results in the modulation of the interfacial injection barrier which governs the resistance state of the device.

Key words:

Memristor, ZnO nanoparticles, Electroabsorption, Oxygen vacancies, F8BT polymer.

1 Present address: Huygens Laboratory, Leiden University, P.O. Box 9504, Leiden 2300 RA, Netherlands.

2 Present address: Institute of Advanced Materials, Nanjing Tech University, Nanjing, 211816, China

a) Authors to whom correspondence should be addressed. Electronic addresses: iamjpwang@njtech.edu.cn or ncg11@cam.ac.uk.

Introduction

Memristors, or resistance switching memories,¹ have been intensely investigated recently,^{2,3} because of their potential applications in next-generation high-density non-volatile memory⁴ as well as artificial synapse-neuron systems.⁵ Although memristive devices have been applied in many different fields, ranging from traditional information technology to biological machine learning systems,^{6,7} the switching mechanism is still not clear. Possible explanations include oxygen ion/vacancy migration,^{8,9} formation/annihilation of conducting filaments¹⁰ and space-charge-limited processes.^{11,12}

Colloidal metal oxide nanoparticles have a number of attractions, including simple synthesis procedure, and compatibility with organic materials.¹³⁻¹⁶ It has been demonstrated that solution-processed colloidal ZnO nanoparticle-based memristive devices exhibit large on/off ratios,¹⁷ which is promising for applications in low-cost memory circuits such as printable radio-frequency identification (RFID) tags.¹⁸ In previous work, Wang *et al.*¹⁷ proposed that the switching mechanism in ITO/ZnO nanoparticle/Al memristors is due to alteration of the barrier at the Al/ZnO interface caused by the drift of oxygen vacancies, combined with the adsorption/desorption of molecular oxygen, under the external electrical field. Although changes in interfacial barriers have been suggested as a possible switching mechanism for metal-oxide-based memristors,^{19,20} direct evidence from experimental observations is still lacking.

Electroabsorption (EA) spectroscopy is a noninvasive technique to investigate the built-in field in metal/insulator/metal (MIM) devices,²¹ and potentially can be useful for studying

the interface barriers in memristors. However, this technique is difficult to apply in metal-oxide-based devices, because their electrical properties can be dramatically changed when metal oxides are excited by the probe light during EA measurement.²² To overcome this problem, we incorporated a small amount of low-bandgap polymer poly(9,9-dioctylfluorene-*co*-benzothiadiazole) (F8BT) as a probe molecule in colloidal ZnO nanoparticle memristors. The absorption peak of F8BT is at a photon energy of around 2.7 eV,²³ which is below the bandgap of bulk ZnO (~3.4 eV).²⁴ Therefore the EA measurement can be performed without disturbing the electrical properties of these ZnO nanoparticle-based devices. Our EA results show that the change of built-in field is consistent with the change of the device resistance state, implying that a modulation of the electrode effective workfunction contributes to the resistance switching in the memristor.

Experimental Methods:

A: Fabrication of the memristor devices

The device structure is glass/ITO/blend of ZnO nanoparticles and F8BT/Al, as shown in inset of Fig. 1(a). These ZnO nanoparticles were synthesized according to a previously reported method with typical size of ~5-6 nm diameter, and were coated with *n*-butyl amine ligands.²⁵ Devices were fabricated by spin-coating a blend of ZnO nanoparticle:F8BT (0.95:0.05 by weight) at 5000 rpm from a chloroform solution (30 mg ml⁻¹) onto patterned ITO coated substrates to form a film of 120 nm thickness, followed by a thermal evaporation of Al (~100 nm) through a shadow mask which

defines the active area of 1 mm×1 mm. During all the electrical experiments, the Al electrode was grounded, and the positive voltage was applied to the ITO layer.

B: Electroabsorption Apparatus

The experimental set-up is shown in Figure 2. A 150 W xenon arc lamp (Oriel 6253) or a 50 W quartz tungsten halogen lamp (Oriel 6332) was used as the light source for the EA experiment. Both light sources were installed with a monochromator illuminator (Newport 7340). A Bruker Optics 250 is/sm monochromator was used to generate a monochromatic probe beam. The sample was mounted within a cryostat (Oxford Instruments, Optistat CF). After reflection from the back contact of the sample (45° incident angle), the probe beam was incident on a silicon photodiode connected via a current-to-voltage converter to a dual-channel lock-in amplifier (Stanford Research Systems SR-830, reference frequency $\omega/2\pi = 2031$ Hz) and a DC voltmeter (HP34401A). The device was driven by a voltage $V_{dc} + V_{ac}\sin(\omega t)$ generated in a summing amplifier circuit using signals from the lock-in amplifier.

Results and Discussion

Fig. 1(a) shows a transmission electron microscopy (TEM) image of ZnO nanoparticles dispersed in the matrix of F8BT polymer on a TEM grid, indicating that there is no significant aggregation in the nanoparticle/F8BT solution. A typical current-voltage (I-V) characteristic under ambient conditions (air) is presented in Fig. 1(b). It shows resistance switching behavior similar to that of typical pure ZnO nanoparticle devices.¹⁷ At forward bias, the device is gradually changed to the high-resistance state (HRS), and it can be recovered by a reverse bias to the low-resistance state (LRS). The ratio of currents in the

high- and low-resistance states can be as large as 5 orders of magnitude at 1.0 V. By decreasing the sweeping speed, the contrast between the LRS and the HRS increases. This dependence on sweeping speed is also similar to that seen in pure ZnO nanoparticle devices¹⁷(Figure S1²⁶). Therefore, the small amount of F8BT incorporated does not significantly affect the memristive performance of the device.

Now we use the device based on a blend of F8BT and ZnO nanoparticles as a model system to investigate the built-in field in the device using EA spectroscopy. EA spectroscopy relies on the modulation of light absorption within a film by an external voltage ($V_{dc}+V_{ac}\sin(\omega t)$). At the fundamental frequency ω , in a film with uniform internal

field, the EA signal $\left. \frac{\Delta R}{R} \right|_{\omega}$ is^{21,27}

$$\left. \frac{\Delta R}{R} \right|_{\omega} \propto \chi^{(3)}(h\nu)V_0V_{ac}\sin(\omega t) = \chi^{(3)}(h\nu)(V_{dc} - V_{BI})V_{ac}\sin(\omega t) \quad (1)$$

where $\chi^{(3)}$ is the third-order electric susceptibility which is a function of photon energy $h\nu$, V_0 is the internal DC voltage, V_{dc} is the external applied DC voltage and V_{BI} is the built-in potential existing in the device. Therefore, by finding the null voltage ($V_{dc}=V_{null}=V_{BI}$) where the EA signal goes to zero, we can directly obtain the built-in potential V_{BI} . In a typical MIM system, where the internal electric field is uniform, the built-in potential V_{BI} is ascribed to the workfunction difference between the top and bottom electrodes.²¹ However, when the electric field distribution is nonuniform due to the accumulation of charges, the electroabsorption signal must be calculated by integrating the electric field through the device, weighted according to the local intensity

of the probe beam.²⁷ Hence, for a device with a reflecting electrode, optical interference of the probe light within the device plays an important role in analysis of the EA signal.

Figure 3(a) shows a series of EA spectra for the ITO/ZnO:F8BT/Al device with increasing external DC bias, together with the absorbance spectrum of a pure F8BT film on a quartz substrate. The EA signal roughly follows the first derivative of the absorption spectrum, consistent with a simple Stark shift of the F8BT *i.e.* transition energy of F8BT associated with the electrical field.²⁸ In order to maximize the signal-to-noise ratio, we selected a photon energy of 2.46 eV to characterize the built-in potential.

Fig. 3(b) shows the EA response at a fixed photon energy of 2.46 eV as a function of DC bias in air. We find that in the forward sweep, the null voltage, V_{null} , applied to neutralize the built-in potential is 0.5 V, consistent with the workfunction difference between Al and ITO electrodes. In the reverse sweep, the built-in potential becomes 1.2 V, implying a shift of the effective workfunction.²⁹ We note that this bias dependent EA signal is not perfectly linear during the sweep. In general, a nonlinearity of EA signal can be ascribed to the movement of mobile charges, associated with a redistribution of the electrical field in the film.³⁰ In reverse bias, there is a roughly parallel shift in the curves between the forward sweep and the early part of the reverse sweep (indicated by the two dashed lines in Fig. 3(b)), implying a change of the built-in field. Comparing with Fig. 1(b), we see that the change in built-in potential correlates with the change of resistance state. The device is in the HRS when V_{BI} is 1.2 V, and in the LRS when V_{BI} is 0.5 V.

Pure ZnO nanoparticle-based devices do not demonstrate significant memristive behavior in the absence of ambient oxygen.^{31,17} The F8BT-doped ZnO nanoparticle device also shows similar effects, as shown in Fig. 4(a). There is no hysteresis in the I-V curves when the device is under vacuum ($\sim 10^{-5}$ mbar). Fig. 4(b) shows EA measurements performed under vacuum. The EA responses in both sweeps are proportional to the external DC voltage with a consistent null voltage of 0.5 V, suggesting that the built-in potential does not change during the sweeps.

Now we discuss the origin of the built-in potential shift and the electrical hysteresis. Since we have found that the Al/ZnO interface is vital for the switching process,¹⁷ we attribute the resistance switching to the formation of a dipole layer at Al/ZnO interface. We start from a pristine device, as shown in Figure 5(a). Once in contact, in order to achieve the equilibrium state, electrons flow from ZnO to the Al electrode until both Fermi levels are aligned, establishing a Schottky barrier.²⁴

When a positive voltage is applied to the ITO layer, as indicated in Fig. 5(b), positively charged oxygen vacancies drift toward the Al/ZnO interface,^{32,33} giving rise to the adsorption of oxygen molecules at these sites of vacancies.^{34,35} This leads to two effects: (1) Occurrence of a charge transfer process, during which electrons flow from conduction band of ZnO to oxygen molecules, resulting in the formation of a interfacial dipole layer.^{36,37} (2) Depletion of the free charge carriers in the ZnO conduction band at the interface, resulting in an increase of the width of the Schottky barrier. In this case, although the height of barrier decreases, the charge injection through the barrier shifts

from a tunneling mechanism to thermionic emission.²⁴ Furthermore, the hopping mechanism dominates the charge transport inside the film, due to the decrease of free charge carrier density caused by adsorbed oxygen molecules. Therefore an interfacial layer is formed giving rise to an increased injection barrier, leading to the HRS as shown in Figure 5(b). This dipole layer, Δ , with a thickness of a few atomic layers,³⁷ effectively decreases the workfunction of Al (Fermi level moves towards to the vacuum level), causing the increase of V_{BI} in the device. Discussion of the effects of probe beam optical interference on the EA signal is presented in the supplementary material (Fig. S2²⁶).

When a negative voltage is applied to the ITO layer, the oxygen vacancies drift away from Al/ZnO interface, leading to a desorption of oxygen molecules at the interface. Without the charge trapping, the free charge carrier density in ZnO nanoparticle films is between 10^{18} cm^{-3} and 10^{19} cm^{-3} ,¹³ and the thickness of the depletion layer is calculated to be around 8 nm. Hence, the tunneling behavior prevails in the charge injection process. Thus the device turns to the LRS, and the built-in potential returns to the simple workfunction difference between the two electrodes, $\sim 0.5 \text{ V}$.

Under vacuum conditions, since the injection barrier does not change (ascribed to the absence of the molecular oxygen adsorption/desorption process), no hysteresis is observed in the I-V curves or in the EA response.

Conclusions

By electrical and EA investigation in both air and vacuum, we have shown evidence that the resistance switching mechanism in ZnO nanoparticle memristors is the drift of oxygen vacancies under the external field, associated with the adsorption and desorption of oxygen molecules at the ZnO nanoparticle/Al interface. This interfacial layer effectively changes the workfunction of Al electrode and results in the modulation of the resistance state. We believe that our findings are important for future memristive device design and fabrication.

Acknowledgements

We are grateful to Auke Jisk Kronemeijer for valuable discussions. Cheng Li acknowledges the Chinese Scholarship Council for financial support. This work was supported by the Engineering and Physical Sciences Research Council [Grant Number [EP/G060738/1](#)].

References

- 1 L. Chua, *Appl. Phys. A* **102**, 765 (2011).
- 2 D. B. Strukov and H. Kohlstedt, *MRS Bulletin* **37**, 108 (2012).
- 3 Y. V. Pershin and M. D. Ventra, *Adv. Phys.* **60**, 145 (2011).
- 4 R. Waser and M. Aono, *Nat. Mater.* **6**, 833 (2007).
- 5 T. Chang, S.-H. Jo, and W. Lu, *ACS Nano* **5**, 7669 (2011).
- 6 M.-J. Lee, C. B. Lee, D. Lee, S. R. Lee, M. Chang, J. H. Hur, Y.-B. Kim, C.-J. Kim, D. H. Seo, S. Seo, U.-I. Chung, I.-K. Yoo, and K. Kim, *Nat. Mater.* **10**, 625 (2011).
- 7 J. J. Yang, D. B. Strukov, and D. R. Stewart, *Nat. Nanotechnol.* **8**, 13 (2013).
- 8 J. J. Yang, M. D. Pickett, X. Li, D. A. A. Ohlberg, D. R. Stewart, and R. S. Williams, *Nat. Nanotechnol.* **3**, 429 (2008).
- 9 I. Kiselev, M. Sommer, V. V. Sysoev, and S. L. Skorokhodov, *Phys. Status Solidi A* **208**, 2889 (2011).
- 10 D. H. Kwon, K. M. Kim, J. H. Jang, J. M. Jeon, M. H. Lee, G. H. Kim, X. S. Li, G. S. Park, B. Lee, S. Han, M. Kim, and C. S. Hwang, *Nat. Nanotechnol.* **5**, 148 (2010).

11 D.-I. Son, D.-H. Park, W. K. Choi, S.-H. Cho, W.-T. Kim, and T. W. Kim,
Nanotechnology **20**, 195203 (2009).

12 D. I. Son, C. H. You, J. H. Jung, and T. W. Kim, Appl. Phys. Lett. **97**, 013304
(2010).

13 G. Lakhwani, R. F. H. Roijmans, A. J. Kronemeijer, J. Gilot, R. A. J. Janssen, and
S. C. J. Meskers, J. Phys. Chem. C **114**, 14804 (2010).

14 S. Foster, C. E. Finlayson, P. E. Keivanidis, Y. S. Huang, I. Hwang, R. H. Friend,
M. Otten, L. Lu, E. Schwartz, R. J. M. Nolte, and A. E. Rowan, Macromolecules
42, 2023 (2009).

15 J. Wang, F. Gao, and N. C. Greenham, Appl. Phys. Lett. **97**, 053301 (2010).

16 F. Verbakel, S. C. J. Meskers, and R. A. J. Janssen, J. Phys. Chem. C **111**, 10150
(2007).

17 J. Wang, B. Sun, F. Gao, and N. C. Greenham, Phys. Status Solidi A **207**, 484
(2010).

18 H. Faber, M. Burkhardt, A. Jedaa, D. Kälblein, H. Klauk, and M. Halik, Adv.
Mater. **21**, 3099 (2009).

19 R. Yang, K. Terabe, T. Tsuruoka, T. Hasegawa, and M. Aono, Appl. Phys. Lett.
100, 231603 (2012).

20 Y. B. Nian, J. Strozier, N. J. Wu, X. Chen, and A. Ignatiev, Phys. Rev. Lett. **98**,
146403 (2007).

21 I. H. Campbell, T. W. Hagler, D. I. Smith, and J. P. Ferraris, Phys. Rev. Lett. **76**,
1900 (1996).

22 Y. Jin, J. Wang, B. Sun, J. C. Blakesley, and N. C. Greenham, Nano. Lett. **8**, 1649
(2008).

23 C. L. Donley, J. Zaumseil, J. W. Andreasen, M. M. Nielsen, H. Sirringhaus, R. H.
Friend, and J. Kim, J. Am. Chem. Soc. **127**, 12890 (2005).

24 S. M. Sze, *Physics of Semiconductor Devices* (Wiley, New York, 1981).

25 C. Pacholski, A. Kornowski, and H. Weller, Angew. Chem. Int. Ed. **41**, 1188
(2002).

26 See supplementary material at [reference link] for the description of the optical
simulation and time dependent current-voltage measurement in the memristor.

27 T. M. Brown, R. H. Friend, I. S. Millard, D. J. Lacey, T. Butler, J. H. Burroughes,
and F. Cacialli, J. Appl. Phys. **93**, 6159 (2003).

28 F. W. Vance, R. D. Williams, and J. T. Hupp, Int. Rev. Phys. Chem. **17**, 307
(1998).

29 I. H. Campbell and B. K. Crone, Appl. Phys. Lett. **88**, 172113 (2006).

30 G. Winroth, O. Fenwick, M. A. Scott, D. Yip, S. Howorka, and F. Cacialli, Appl.
Phys. Lett. **97**, 043304 (2010).

31 F. Verbakel, S. C. J. Meskers, and R. A. J. Janssen, J. Appl. Phys. **102**, 083701
(2007).

32 A. Shih, W. Zhou, J. Qiu, H.-J. Yang, S. Chen, Z. Mi, and I. Shih,
Nanotechnology **21**, 125201 (2010).

33 J. J. Yang, F. Miao, M. D. Pickett, D. A. A. Ohlberg, D. R. Stewart, C. N. Lau,
and R. S. Williams, Nanotechnology **20**, 215201 (2009).

34 Z. Liao, K. Liu, J. Zhang, J. Xu, and D. Yu, Phys. Lett. A **367**, 207 (2007).

- ³⁵ Z. Fan, D. Wang, P. Chang, W. Tseng, and J. Lu, Appl. Phys. Lett. **85**, 5923 (2004).
- ³⁶ G. Heiland and P. Kunstmann, Surf. Sci. **13**, 72 (1969).
- ³⁷ M. W. Allen and S. M. Durbin, Appl. Phys. Lett. **92**, 122110 (2008).

Figure captions:

FIG. 1. (a) Plan-view bright-field transmission electron microscopy image of ZnO nanoparticles embedded in an F8BT layer on a TEM grid. Inset: Schematic device structures. (b) Current-voltage characteristics (I-V) of the device in air. The arrows indicate the direction of applied voltage sweeps. The sweeping speed is 0.1 V s^{-1} .

FIG. 2. Schematic diagram of an electroabsorption spectroscopy system, in which a combination of DC and AC voltages is applied to the device, and the lock-in amplifier is used to measure the AC component, ΔR , of light reflected from the device.

FIG. 3. (a) Bias dependence of first harmonic EA spectra for an ITO/ZnO:F8BT/Al device (black lines) and the absorption spectrum for a pure F8BT film spin-coated on a quartz substrate (red dashed line). The dotted line indicates the photon energy, 2.46 eV, for the EA measurement. (b) DC bias dependence of EA response under ambient air conditions, showing forward and reverse sweeps. ε indicates the shift of the null voltage between the two sweep directions. The dashed lines are shown as a guide for the eye to indicate the shift of the built-in field.

FIG. 4. (a) Current-voltage characteristics of the memristor under vacuum conditions. The sweeping speed is 0.1 V/s . (b) EA response vs DC bias for forward and reverse sweeps in vacuum. The arrows indicate the directions of applied voltage sweeps. To avoid destroying the device by a high current, the sweep range was limited to between -2 V and 2 V .

FIG . 5. (a) Schematic energy band diagram (not to scale) of the memristor in the low-resistance state. (b) Band diagram in the high-resistance state, showing the influence of oxygen vacancies under ambient air conditions. W and δ indicate the width of the Schottky barrier and the dipole layers, respectively. χ represents the electron affinity of the ZnO layer, Φ_m is the workfunction of the Al electrode, and Δ is the voltage dropped across the dipole layer.

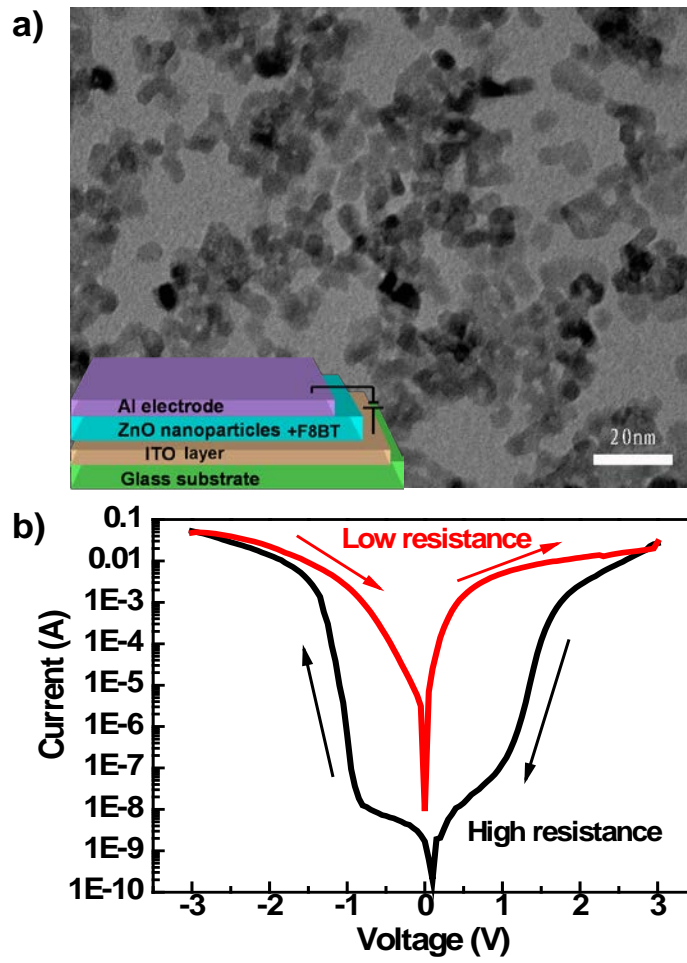


Figure 1.

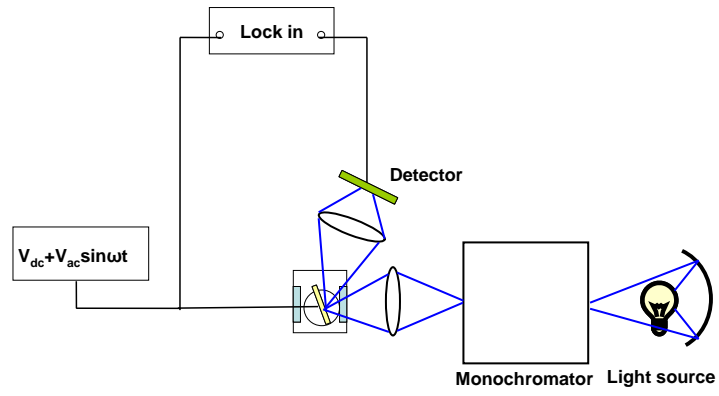


Figure 2.

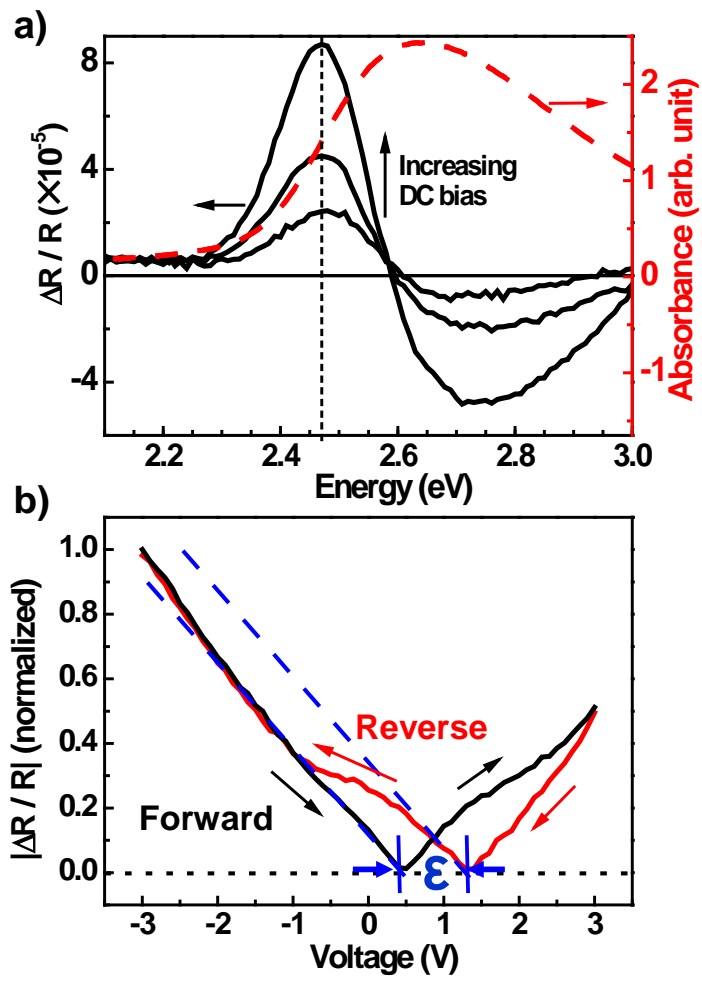


Figure 3.

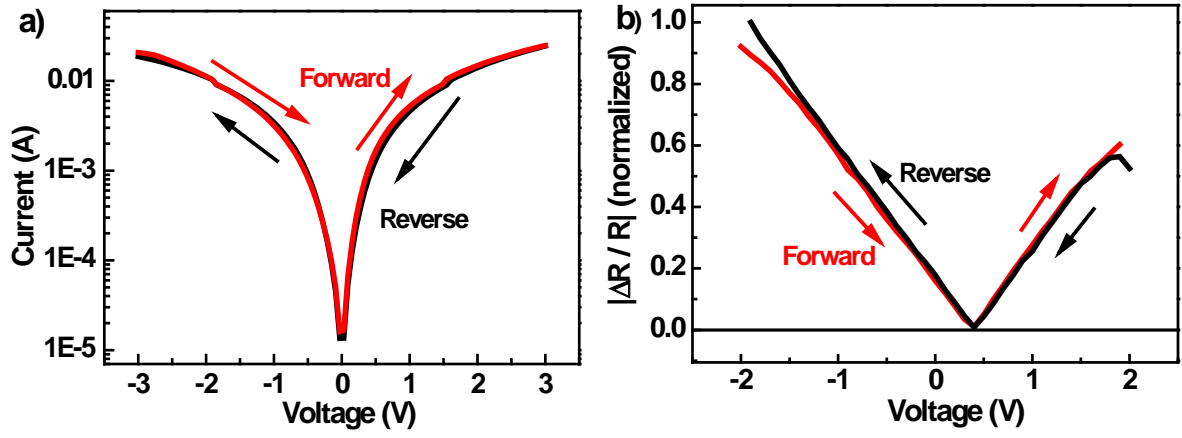


Figure 4.

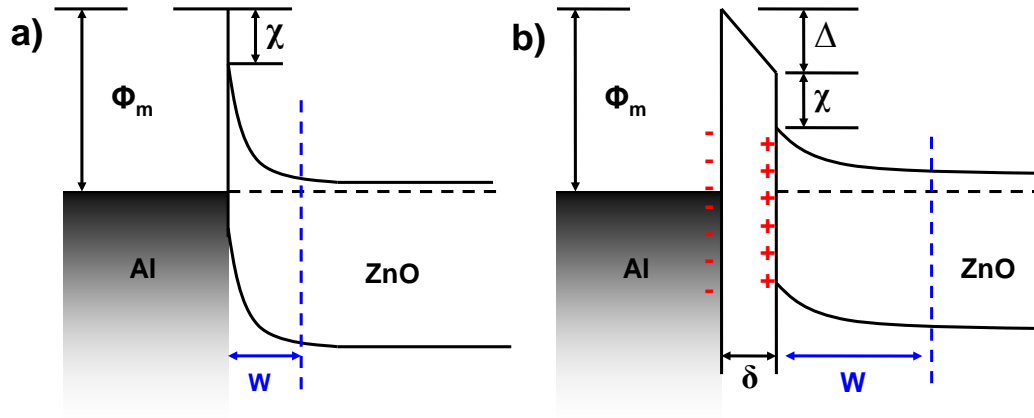


Figure 5.